Physica Medica 33 (2017) 47–55

Contents lists available at ScienceDirect

Physica Medica

journal homepage: http://www.physicamedica.com

Original paper

A feasible and automatic free tool for T1 and ECV mapping

Luisa Altabella [a,*], Cristian Borrazzo [a,c], Marco Carnì [a], Nicola Galea [b], Marco Francone [b], Andrea Fiorelli [b], Elisabetta Di Castro [a,c], Carlo Catalano [b], Iacopo Carbone [b]

[a] Medical Physics Unit, Policlinico Umberto I, Rome, Italy
[b] Department of Radiological, Oncological and Pathological Sciences, University of Rome La Sapienza, Rome, Italy
[c] Department of Molecular Medicine, University of Rome La Sapienza, Viale Regina Elena 291, 00161 Rome, Italy

ARTICLE INFO

Article history:
Received 15 February 2016
Received in Revised form 28 October 2016
Accepted 4 December 2016
Available online 18 December 2016

Keywords:
Cardiac magnetic resonance
T1 mapping
ECV mapping
Myocardial fibrosis

ABSTRACT

Purpose: Cardiac magnetic resonance (CMR) is a useful non-invasive tool for characterizing tissues and detecting myocardial fibrosis and edema. Estimation of extracellular volume fraction (ECV) using T1 sequences is emerging as an accurate biomarker in cardiac diseases associated with diffuse fibrosis. In this study, automatic software for T1 and ECV map generation consisting of an executable file was developed and validated using phantom and human data.

Methods: T1 mapping was performed in phantoms and 30 subjects (22 patients and 8 healthy subjects) on a 1.5T MR scanner using the modified Look-Locker inversion-recovery (MOLLI) sequence prototype before and 15 min after contrast agent administration. T1 maps were generated using a Fast Nonlinear Least Squares algorithm. Myocardial ECV maps were generated using both pre- and post-contrast T1 image registration and automatic extraction of blood relaxation rates.

Results: Using our software, pre- and post-contrast T1 maps were obtained in phantoms and healthy subjects resulting in a robust and reliable quantification as compared to reference software. Coregistration of pre- and post-contrast images improved the quality of ECV maps. Mean ECV value in healthy subjects was 24.5% ± 2.5%.

Conclusions: This study demonstrated that it is possible to obtain accurate T1 maps and informative ECV maps using our software. Pixel-wise ECV maps obtained with this automatic software made it possible to visualize and evaluate the extent and severity of ECV alterations.

© 2016 Associazione Italiana di Fisica Medica. Published by Elsevier Ltd. All rights reserved.

1. Introduction

Cardiac magnetic resonance (CMR) imaging has grown rapidly over the past decades and has been established as a reliable and robust technique for assessing cardiac morphology, function, perfusion and tissues [1]. In particular, late gadolinium enhancement (LGE) imaging has been affirmed as the reference standard for non-invasive *in-vivo* assessment of myocardial necrosis, fibrosis and scarring [2,3], which appear hyperintense on MR images due to gadolinium accumulation compared to the null signal from adjacent healthy myocardium.

The LGE technique is highly reliable and robust in the detection of "focal" myocardial damage, but it is extremely weak in the assessment of diffuse involvement [4]. Diffuse myocardial fibrosis due to increased collagen deposition and fibroblast proliferation leads to wall stiffness, abnormal contractility and arrhythmia and constitutes a common endpoint for a wide variety of cardiomyopathies. Early detection could be of great benefit to patient risk stratification [5].

A quantitative and reproducible method for assessing diffuse fibrosis is offered by the new T1 mapping technique, which quantifies pre- and post-contrast myocardial longitudinal relaxation time. However, the absolute measure of post-contrast T1 is influenced by several factors, such as variations in the time elapsed between contrast injection and image acquisition, contrast dose, body weight, gadolinium clearance (which depends on the renal function) and hematocrit [6].

Estimation of extracellular volume fraction (ECV) defined as the proportion of myocardium occupied by extracellular space has emerged as an accurate and reproducible method for depicting myocardial fibrosis subsequently confirmed by histological outcome [6,7].

ECV can be calculated easily starting from the partition coefficient of the myocardium and blood cavity measured before and after contrast agent injection at an equilibrium phase corrected for hematocrit. Manual ECV quantification is carried out by

* Corresponding author at: Medical Physics Department, Ospedale San Raffaele, Milan, Italy.
E-mail address: luisa.altabella@gmail.com (L. Altabella).

http://dx.doi.org/10.1016/j.ejmp.2016.12.002
1120-1797/© 2016 Associazione Italiana di Fisica Medica. Published by Elsevier Ltd. All rights reserved.

manually drawing regions of interest (ROIs) within the myocardium and blood cavity in the pre- and post-contrast T1 maps. It is easily performed, but it does not provide any quantitative data or information on fibrosis distribution. The automatic generation of ECV maps using pixel-wise computation of ECV values on each voxel has been proposed in experimental studies. This method provides a direct graphic representation of the extension and severity of myocardial fibrosis as well as an anatomical assessment of the involved segments and analysis of transmural pattern distribution [6,8]. However, ECV mapping is laborious and time consuming and requires correction of coregistration errors due to heart displacement between the images, which may be caused by patient movement, irregularity of the heart rate and/or inadequate breath-hold [6].

The purpose of this study was to develop and validate a practical tool with an intuitive and simple graphic interface for automatic ECV map creation using a fluent data processing flow.

2. Materials and methods

2.1. Phantom study

Before the *in-vivo* application of our software, the T1 mapping algorithm was tested using a known reference standard. Eight phantoms were built with different T1 values ranging from 250 to 1000 ms and with a T2 value similar to that of the myocardium (about 50 ms). The phantoms consisted of tubes filled with 2% agarose gel (Sigma-Aldrich©) with different concentrations of CuSO4 (Sigma-Aldrich©) (from 0.25 to 2 mM). An additional phantom was built to simulate pre-contrast blood pool T1 and T2 (1500 ms and 200 ms, respectively) [9].

2.2. Human study

A total of 30 subjects, 22 consecutive patients referred to CMR for known or suspected heart disease and 8 healthy volunteers were prospectively enrolled and studied on a 1.5T MR scanner (Magnetom Avanto, Siemens Healthcare, Erlangen Germany). The patients were referred for the following reasons: suspected myocarditis (10 patients), hypertrophic CMP (2 patients), dilated CMP (2 patients), non-compacted CMO (2 patients), pulmonary hypertension (2 patients), other cardiac conditions (4 patients).

All procedures followed were in accordance with the ethical standards of the responsible committee on human experimentation (institutional and national) and with the Helsinki Declaration of 1975, as revised in 2000. Written informed consent was obtained from all patients and volunteers included in the study.

2.3. Image acquisition

Phantoms were scanned using a modified Look-Locker inversion-recovery (MOLLI) prototype sequence (provided by Siemens). MOLLI sequence parameters were the following: matrix 218×256, voxel size $1.41 \times 1.41 \times 8\ mm^3$, TR/TE 2.6/1.12 ms, FA 35°. For pre-contrast acquisitions the protocol was 5(3)3 consisting of 2 inversions with 5 images after the first inversion, a 3-heartbeat pause and then the last 3 images. For post-contrast acquisitions, the protocol was 4(1)3(1)2 consisting of 4 images acquired after the first inversion pulse and a one-heartbeat pause for the complete recovery of magnetization. Then 3 and 2 images, respectively, were acquired after the second and third inversion, separated by a one-heartbeat pause. Two different sequence schemes were used for pre- and post-contrast acquisitions [10].

For a reliable ECV mapping, slice position, field of view and matrix have to be identical in pre- and post-contrast acquisitions. In phantoms, MOLLI acquisitions were performed using a simulated heart rate (HRs) of 60 beats per minute. The *in-vivo* study used MOLLI sequences with the same parameters as those used for the phantom study. In each subject 3 slices were acquired on short axis views in basal, mid-ventricular and apical positions before and 15 min after intravenous bolus injection of 0.1 mmol/kg of gadobenate dimeglumine (Gd-BOPTA; Multihance©, Bracco, Milan, IT).

All MOLLI images were automatically processed for motion correction using a dedicated algorithm [11] incorporated in the scanner.

2.4. Image analysis

Images were analyzed using the developed tool (see next paragraph for details). The proposed T1 fitting methods were compared to a well-established free software, MRmap [12]. This software uses a different algorithm for T1 fitting as explained below. T1 maps obtained with our fitting algorithm from phantom and healthy subject data were compared with those obtained using MRmap considering T1 values extracted from the same ROI. Validation on phantoms is crucial in order to avoid confounding factors due to movements, field inhomogeneity and low SNR and to exploit a wide range of T1.

2.5. Software description

The entire computational system for T1 mapping and ECV mapping consists of an executable file developed in MATLAB (Mathworks Inc.). Initially, salt-and-pepper noise was removed from MOLLI images using a median filter and a threshold mask with a variable cut-off to avoid pixels with random noise. The Fast Nonlinear Least Squares (FNLS) algorithm was implemented in order to obtain a rapid and robust fitting of MOLLI images. Pixel-wise parametric mapping was performed applying a curve fit to the multiple inversion time measurements obtained with MOLLI sequences.

Mathematically, each fit is required to estimate non-linear parameters from the following curve fitting model

$$S(x,\ y,\ t_i) = A(x,\ y) + B(x,\ y) \cdot \exp\left(-\frac{t_i}{T1^*(x,\ y)}\right) \tag{1}$$

and estimate in each (x, y) voxel the non-linear parameters $A(x, y)$ $B(x, y)$ and $T1^*(x, y)$ that best fit the data. Here data is the signal $S(x, y, t_i)$ of the image in a specific voxel (x, y) acquired with a specific t_i. This model can be generalized as:

$$y_i = f(\beta,\ t_i) \tag{2}$$

where y_i is the signal in one location at different inversion times t_i, (i = 1, ...n), β is the vector containing the parameters to be estimated. The aim was to find the β that best fitted the data in the least squares sense, defined as the sum of squares. For any choice of β, the residuals can be computed as follows:

$$\epsilon_i = y_i - f(\beta,\ t_i) \tag{3}$$

This means to minimize the $S = \sum_{i=1}^{m} \epsilon_i^2$, sum of the residuals, setting its derivative equal to zero:

$$\frac{\partial S}{\partial \beta_j} = 2\sum\nolimits_i \epsilon_i \frac{\partial_i}{\partial \beta_j} = 0 \tag{4}$$

Several different methods provide a solution to this non-linear least squares problem. For example, many T1 mapping tools including MRmap solve this problem using the Levenberg-Marquardt method [12,13]. In this study, we considered a reduced dimension approach for solving Eq. (4), which permits separation of the unknown variables in S as already proposed by Barrel

et al. [15]. Noise has a different effect on each sample point of the recovery curve which presents a different SNR because it is acquired using a different inversion time. For this reason, a weighted total least squares using the geometric fitting procedure was applied to minimize the orthogonal distance to the curve [14]. This requires minimization of a weighted sum $S = \sum_{i=1}^{m} W_i \epsilon_i^2$ of squares. The expression implies that the squared residuals (measured value minus estimated model value) are multiplied by weights. To satisfy the requirements of fitting, the weights W_i should be related to the standard error σ_{yi} of the measurements by $W_i = 1/\sigma_{yi}$. As the uncertainties are normally distributed, the assumption that the weights are the inverse of the variances means that the best fitting value is equivalent to the maximum likelihood estimation. In MR images the correct model for implementing the T1 fitting is:

$$S(t_i) = e^{i\phi} \cdot \left(r_a + r_b \cdot e^{-\frac{t_i}{T1^*}} \right) \tag{5}$$

where Φ is the phase of the constant which receives contributions from T2 and coil sensitivity [15]. This model has four unknown real-valued parameters for estimating Φ, r_a, r_b, and $T1^*$. In magnitude fit the polarity needs to be restored in order to use real-valued parameters. This means to find the time τ with null signal to switch the sign of points acquired with inversion times lower than τ. Time value τ that defines the zero crossing is defined as:

$$r_a + r_b \cdot e^{-\frac{\tau}{T1}} = 0 \tag{6}$$

This operation is carried out to determine τ, but it is computational time consuming. To overcome this, the same problem in Eq. (6) can be represented differently using complex parameters. It can be written as follows:

$$S(t_i) = A + B \cdot e^{-\frac{t_i}{T1^*}} \tag{7}$$

where A and B are complex parameters defined as $A = r_a e^{i\Phi}$ and $B = r_b e^{i\Phi}$. This model represents an overparameterization of the first model, because it requires estimation of five parameters: the real and imaginary parts of both A and B ($Re\{A\}$, $Re\{B\}$ and $Im\{A\}$ and $Im\{B\}$), and $T1^*$. Fitting complex data to a five-parameter model ensures accuracy of the T1 estimation, but it is usually a time consuming fitting procedure [15]. For this reason, a reduced dimension complex fitting procedure as proposed by Barral et al. [15] was also considered. Both fitting types (magnitude and complex) were implemented to find the best solution for the T1 mapping procedure. It is well-known that the fitting procedure as well as the number of estimated parameters can affect the accuracy of T1 determination [10]. The plots of the mean residuals of the fitting and the corresponding Gaussian fitting were also obtained and are shown in the Section 3. Finally the Look Locker correction [10] was applied in order to avoid the effect of readout on T1 determination:

$$T1 = \left(\frac{B}{A} - 1 \right) \cdot T1^* \tag{8}$$

In the healthy subjects, ROIs were manually positioned on the myocardium, septum and lateral wall and compared to native T1 values reported in the literature [16]. Performance of the FNLS fitting algorithm was measured using a 2.9 GHz Intel Core i7 processor with 8 GB of RAM.

After the pre- and post-contrast T1 mapping procedure, ECV mapping can be carried out by calculating pixel-by-pixel ECV from the reciprocal pre- and post-contrast T1 values applying the following formula:

$$ECV_{myo}(\%) = (1 - h) \cdot \left(\frac{\Delta R_{myo}}{\Delta R_{blood}} \right) \cdot 100 \tag{9}$$

where $\Delta R_{myo} = \frac{1}{T1_{post}} - \frac{1}{T1_{pre}}$ stands for myocardium, $\Delta R_{blood} = \frac{1}{T1_{post}} - \frac{1}{T1_{pre}}$ for blood pool and h is the hematocrit, which can be considered the proportion of the intracellular space of blood. Factor $(1 - h)$ converts the equation from a partition coefficient calculation to myocardial ECV. For the ECV mapping, pre- and post-contrast myocardial relaxation rates were derived pixel-wise from pre- and post-contrast T1 maps, whereas the blood pool mean values were considered both in pre- and post-contrast maps. The standard approach for manual ECV calculation, which does not produce a visual map, uses mean values from myocardial pre- and post-contrast T1 maps. In order to obtain reliable and automatic ECV maps, several steps are implemented in our software. First of all, pre- and post-contrast T1 maps are coregistered in order to avoid misregistration between the two maps, as this can affect the quality of the ECV map. Misregistration may be caused by possible patient position variations between pre- and post-acquisitions and/or small changes in the respiratory phase. The complexity of image coregistration in MOLLI acquisitions depends on the different image contrast within the series due to the different acquisition inversion times [11]. To overcome this critical point, image coregistration is implemented in our software using affine image registration between the pre- and post-contrast images with the longest inversion time when all spins are relaxed as proposed by Kellman et al. [6]. An intensity-based image registration method can then be used to directly estimate the mapping transformation from the observed image intensities of the two images by solving a minimization problem defined through an iterative process. The affine image registration used allows translation, rotation, scale and shear, which are necessary because of the intrinsic non-rigid heart movements. Finally, transformation of post-contrast image to pre-contrast image was applied to the post-contrast T1 map.

The second step implemented to obtain operator independent ECV maps is an automatic mask designed to obtain blood pool relaxation rate for pre- and post-contrast T1 maps. In order to avoid most of the pixels outside the heart, the user can select a rectangular region that includes all the myocardium. This is possible by clicking, in the upper left and lower right corners of the rectangle that includes the heart on the pre-contrast T1 map. A pixel threshold greater than 1250 ms is subsequently applied to this selected region on pre-contrast T1 maps. Blood presents higher T1 values than other tissues [6]. The obtained mask is then corrected for partial volume effects that may affect myocardium-blood edge using a filter. The values for pre- and post-contrast blood pool T1 were calculated as the median of all values of the T1 map identified by the mask. In this study, the post-contrast T1 map was located in the same position as the pre-contrast T1 map thanks to coregistration. Automatic calculation of blood pool T1 values were compared with values from manually drawn ROIs to test the robustness of this automatic approach. After these pre-processing steps, ECV maps could be generated. Hematocrit of the human subjects can be inserted by the operator.

In order to validate our ECV mapping software, our map values were compared to those obtained using the standard approach to ECV calculation, i.e. manual drawing of ROIs in the pre- and post-contrast T1 maps and application of formula (9) for ECV calculation as previously explained. Manual segmentation of the myocardium was used to obtain myocardial ECV values. Manual segmentation was automatically applied both in pre- and post-contrast T1 maps to obtain native and post-contrast T1 values in the same myocardial regions in order to eliminate differences due to different segmentation between automatic and manual ECV calculation. Pre- and post-contrast blood pool T1 values for the manual calculation of ECV were obtained drawing a ROI in the blood pool of the pre- and post-contrast T1 maps.

Myocardial ECV values obtained both using and not using pre- and post-contrast image registration were compared to evaluate the influence of coregistration in ECV mapping.

2.6. Statistical analysis

All continuous variables are expressed as their mean and standard deviation. Variables estimated through fitting procedures are expressed as the parameter value, and uncertainty is expressed as propagation of uncertainty. Comparison between two means was performed using two-sided paired *t*-tests with $p < 0.05$ considered statistically significant in all analyses. Correlation between measurements was tested using Pearson's linear correlation coefficient, where *r* and *p* values are provided. Bland-Altman analysis and graphs were used to compare results from different software (ECVmap and MRmap) and they were computed using Graph Pad Prism 6 (GraphPad Software, La Jolla California USA, www.graphpad.com).

3. Results

3.1. Phantom study

In the first part of the study, the software was tested on phantoms. Fig. 1 shows an example of a T1 map obtained by scanning the phantoms with MOLLI sequences and subsequent reconstruction using our software.

T1 maps obtained in phantoms were compared to those obtained using MRmap. Bland-Altman plots for phantom data are shown in Fig. 3a. A bias of 0.0014 and a confidence interval (CI) between −0.006 and 0.009 ms were found.

Mean residuals representing the distance between the experimental and corresponding points on the fitting are considered for both pre- and post-contrast MOLLI acquisition schemes. Gaussian curve fittings yielded full width at half maximum (FWHM) values comparable to both pre- and post-contrast T1 values (2.01 and 2.38, respectively, see Fig. 4a and b).

No differences related to the phantom data were reported using the complex or magnitude fitting procedure in the entire T1 range.

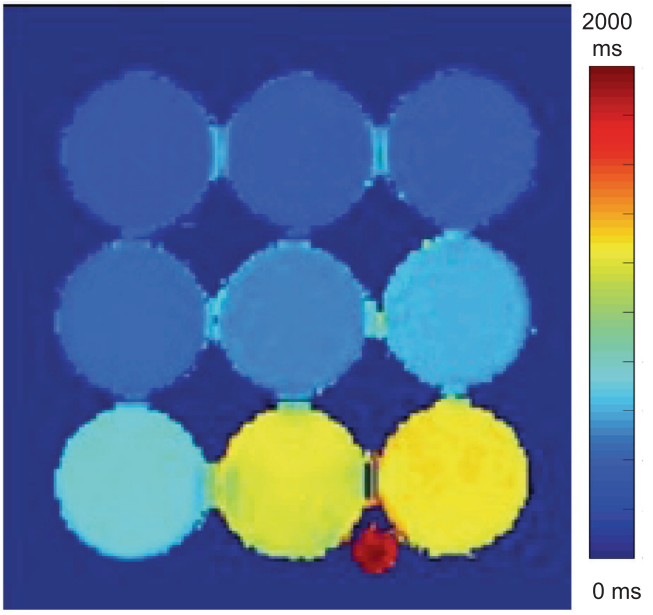

Fig. 1. An example of T1 map for phantom acquired using MOLLI sequence and processed with using FNLS algorithm.

3.2. Human study: T1 mapping

The software was then tested on *in vivo* data from healthy subjects. Using the complex method to fit the pre-contrast data, a mean myocardial T1 value of 1012 ± 48 ms was found in close agreement with the MRmap value (1015 ± 54 ms) as reported also using the Bland-Altman analysis (bias = 2.9 ms and CI between −6.8 and 12.7 ms, see Fig. 3b). Using complex fitting on post-contrast images, the healthy subjects presented higher post-contrast blood pool T1 values with respect to complex fitting (T1 = 304 ± 33 ms with magnitude fitting and T1 = 365 ± 10 ms with complex fitting, $p < 0.001$). The blood pool T1 values are important for an accurate ECV calculation (see formula (10)). To establish the correct post-contrast blood pool T1 values, these T1 values were compared to those obtained using MRmap (T1 = 301 ± 39 ms). Analysis showed that magnitude fitting used for the post-contrast dataset resulted in blood pool T1 values comparable to the reference standard ($p = 0.89$), whereas complex fitting yielded results statistically different from the reference standard ($p < 0.001$). Finally, Bland–Altman analysis of post-contrast myocardial values resulted in bias = 0.16 ms with CI between −4.4 and 4.1 ms in post-contrast images (see Fig. 3c).

An example of pre- and post-contrast T1 maps obtained using complex and magnitude fitting, respectively, is shown in Fig. 2.

As to the *in vivo* data, Gaussian fitting of the mean residuals showed a FWHM comparable to both pre- and post-contrast T1 values (11.47 and 11.75, respectively). In Fig. 4, mean residuals of phantom and human data both in pre- and post-contrast MOLLI acquisitions are shown.

Table 1 shows the mean pre- and post-contrast T1 values in the entire myocardium, septum and lateral wall in healthy subjects. No significant differences were found in pre- and post-contrast T1 values the in septum and lateral wall compared to the entire myocardium ($p = 0.22$ and $p = 0.17$, respectively).

The two fitting procedures differ in terms of computational velocity. Table 2 shows times (in *s*) required for magnitude and complex fitting using different masks.

Validation using MRmap was also performed on the patient data. A strong correlation with MRmap was found in both pre- and post-contrast datasets. A bias of 0.6 ms and CI between −7.2 ms and 8.4 ms was found in native T1 images, and a bias of 0.95 ms and CI between −4.5 ms and 6.4 ms was found in post contrast dataset.

3.3. Human study: ECV mapping

The new software designed for ECV mapping was tested in both healthy subjects and patients. An example of ECV map obtained in a healthy subject is shown in Fig. 5. The mean ECV value found in the healthy subjects was 24.5% ± 2.5%.

As explained in Section 2, the binary mask using a pixel threshold greater than 1250 ms in pre-contrast T1 maps is applied on a selected region of the image that includes the entire myocardium. Considering all slices obtained in all the subjects (8 healthy subjects and 22 patients), comparing automatic blood pool T1 values using the mask with those obtained with manual segmentation, a significant correlation in both pre- (automatic T1 values = 1404 ± 83 ms, manual T1 values = 1440 ± 104 ms, $r = 0.92$ $p < 0.001$) and post- (automatic T1 values = 332 ± 43 ms, manual T1 values = 329 ± 44 ms, $r = 0.91$ $p < 0.001$) contrast datasets was found. Subsequently, the myocardium ECV values obtained in healthy subjects and patients were tested. In myocardium ECV values calculated using the two approaches, a significant correlation (automatic ECV values = 31.72% ± 7% manual ECV values = 34.82% ± 8.6%, $r = 0.81$ $p < 0.001$) was found.

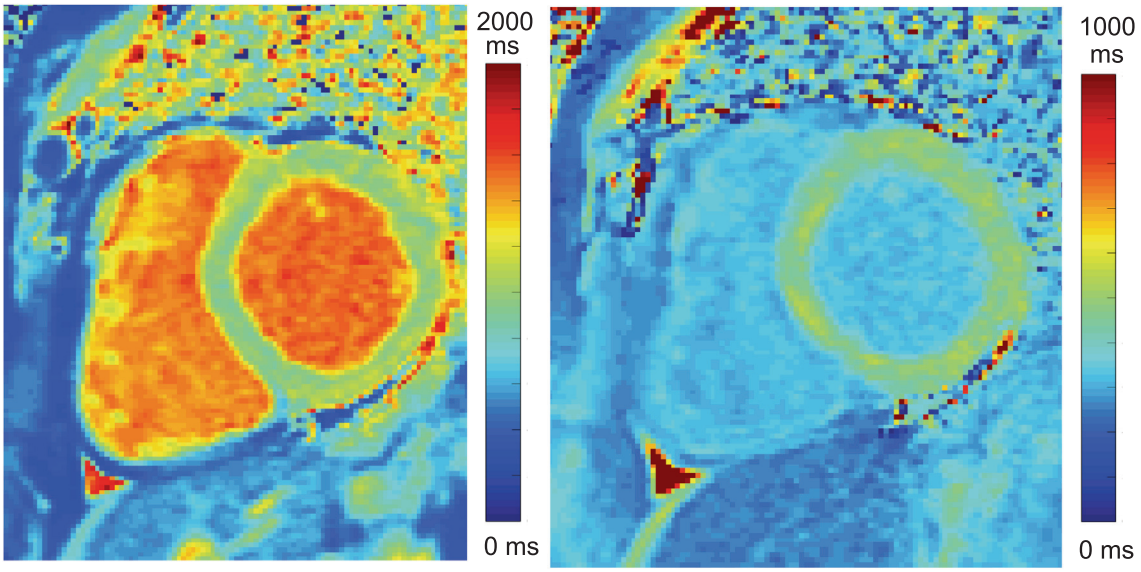

Fig. 2. On the left the pre-contrast T1 map for a healthy subject using complex fit is shown. On the right the corresponding post-contrast T1 map using magnitude fit.

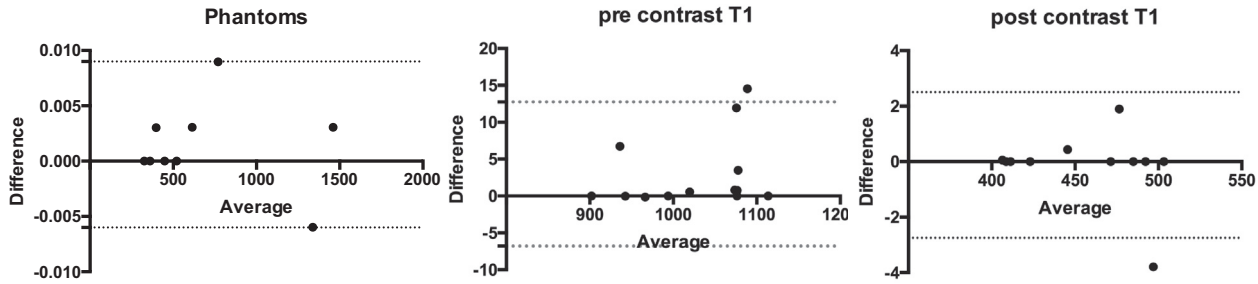

Fig. 3. Bland-Altman plots show the agreement between our T1 fitting results and MRmap for phantoms, pre- and post-contrast healthy subject images respectively. The 95% confidence interval limits of agreement are displayed. All values are presented as differences (ms).

Coregistration between pre- and post-contrast images yields significantly different ECV values compared to not coregistered data ($p < 0.01$). Fig. 6 shows a box plot of ECV values obtained in 8 healthy subjects with and without coregistration between pre- and post-contrast maps and an example of coregistered and not coregistered maps. The quality of the ECV map is improved using our affine coregistration.

Finally, the patient group was retrospectively evaluated and 11 out of 22 patients presented LGE areas. In these patients, the LGE+ areas and LGE− areas in the interventricular septum were segmented. Native T1, post-contrast-T1 and ECV values in LGE+ vs LGE− areas within the septum presented significant differences. The results are summarized in Table 3.

4. Discussion

In this study a new tool for T1 mapping and ECV mapping is presented. In T1 mapping, the FNLS fitting algorithm was implemented using both complex and magnitude procedures that were tested on phantoms and human data. Phantom data were used as reference standard to test the accuracy of the method. Two different MOLLI sequence schemes were used in pre- and post-contrast scans: the first increases the accuracy of T1 measurements in high T1 value tissues, such as native myocardial T1, whereas the second scheme is more accurate in low T1 value tissues, e.g. post-contrast acquisitions [10]. In deed, in pre-contrast images fewer points were acquired because T1 values were higher and consequently the recovery curve was less steep. For this reason, the eight points sampled during recovery of magnetization were distributed along the entire inversion time interval (i.e. from 100 to 3000 ms). However, after contrast agent injection, T1 of blood pool and tissues decreased and recovery of magnetization was fast. This required sampling of more points in a short inversion time, and therefore also before the zero crossing. In order to test the robustness of the fitting algorithm, T1 maps obtained were compared to those generated using a reference software, MRmap [12].

Furthermore, no differences are reported using complex fitting and magnitude fitting on the phantom datasets. In the phantom data all points were well fitted, as suggested by Fig. 3 where mean fitting residuals are shown.

In the second part, the FNLS T1 map fitting algorithm was validated on healthy subjects. The *in vivo* data present some critical points compared to the phantoms, such as movements caused by heart beat and breath and different magnetic susceptibility leading to reduced magnetic field homogeneity and physiological variations *in vivo* [19]. In the data analysis, apical slices were not considered because these slices are strongly affected by partial volume error caused by imperfect orthogonal slice positioning with respect to the heart axis.

As shown in the Section 3, fast, robust and reliable T1 maps were obtained using complex fitting of pre-contrast maps and

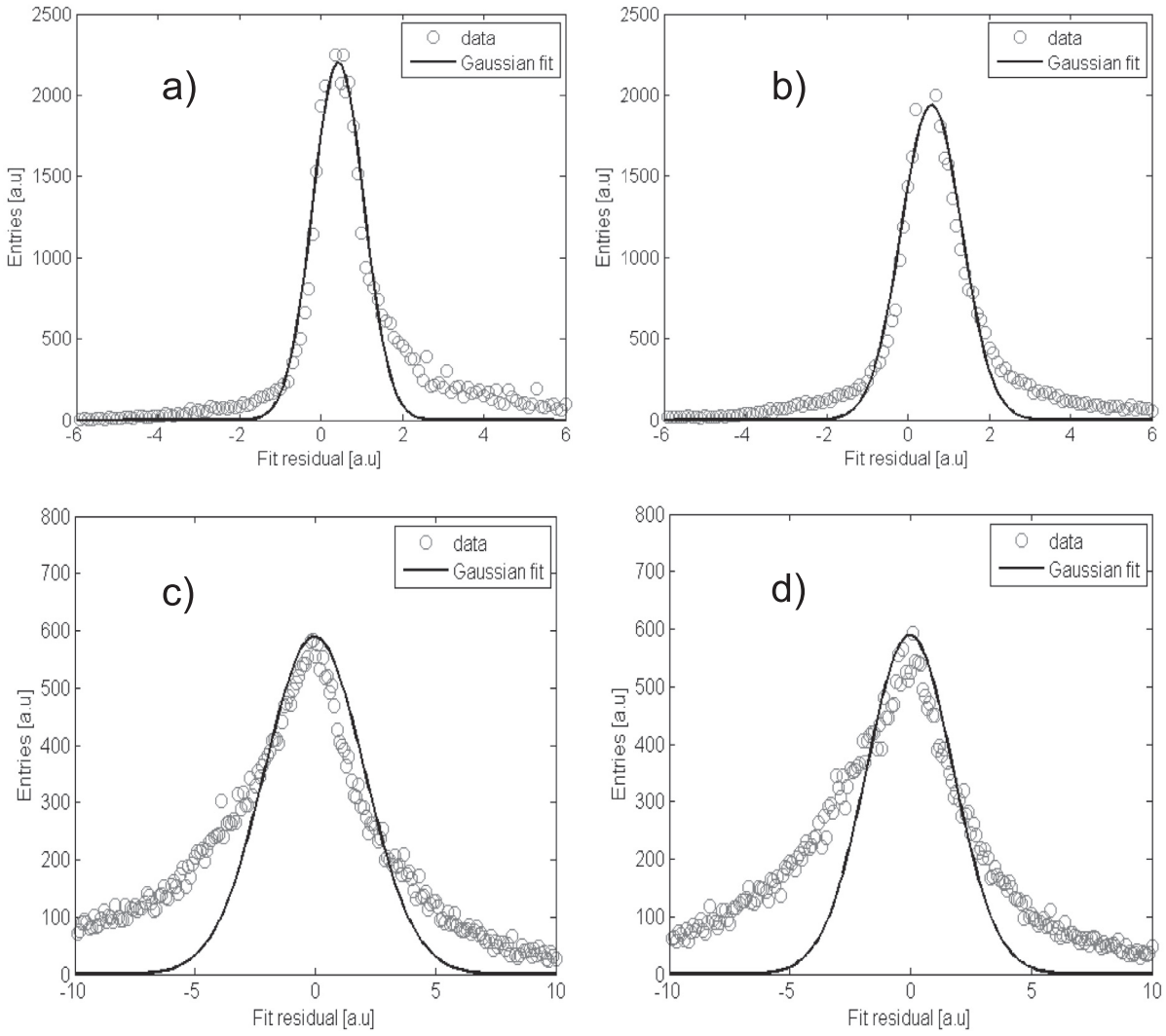

Fig. 4. The mean residual plots and their Gaussian fits both for phantom (panels a) for pre-contrast acquisition scheme and b) for post-contrast acquisition scheme) and healthy subjects (panels c) for pre-contrast images and d) for post-contrast images) are shown in figure.

Table 1
Mean pre-and post-contrast T1 values (±SD) for ROI placed in whole myocardium, septum and lateral wall for healthy subjects are reported in table. No significant differences in mean T1 values are found between myocardial regions compared to whole myocardium (p = 0.22 for septum and p = 0.17 for lateral wall).

	Pre contrast T1 values (ms)	Post contrast t1 values (ms)
Whole Myocardium	1012 ± 48	461 ± 33
Septum	997 ± 45	470 ± 36
Lateral wall	994 ± 36	474 ± 33

Table 2
Computational velocity (s) for magnitude and complex fitting considering different threshold are shown in table. Time values are obtained using a 2.9 GHz Intel Core i7 processor with 8 GB of RAM.

Threshold value	Number of fitted voxels	Complex fitting (s)	Magnitude fitting (s)
0.05	31,080	33	66
0.005	46,143	48	93
0.0005	51,402	54	107

magnitude fitting of post-contrast T1 maps. Complex fitting of high T1 values provides fast and reliable native T1 maps compared to the reference software MRmap, but also compared to the MOLLI sequence values reported in the literature [16,17]. However, the use of this fitting procedure on post-contrast data led to an overestimation of the blood pool post-contrast T1, which considerably affected the ECV calculation.

In order to validate the proposed T1 fitting, results obtained using our new fitting algorithm were compared to the maps obtained using an already validated software for T1 mapping such as MRmap. In comparison with MRmap software, which uses the Levenberg-Marquardt method to solve the non-linear least square problems, our fitting method is reliable and robust both on phantoms and *in vivo* data. The CIs of the two methods both in pre- and post-contrast datasets are significantly reduced compared to the errors in T1 measurements using MOLLI sequence. As example, considering the highest bias (2.9 ms) and CI (about 20 ms) found for pre-contrast dataset, they are lower compared to the error of T1 mapping technique itself (see i.e. Ref. [18]). Indeed, MOLLI sequence underestimates T1 of about 8–10% at high T1 values (around 1000 ms), while differences between algorithms are less than 2% for these T1 values. The strong agreement between

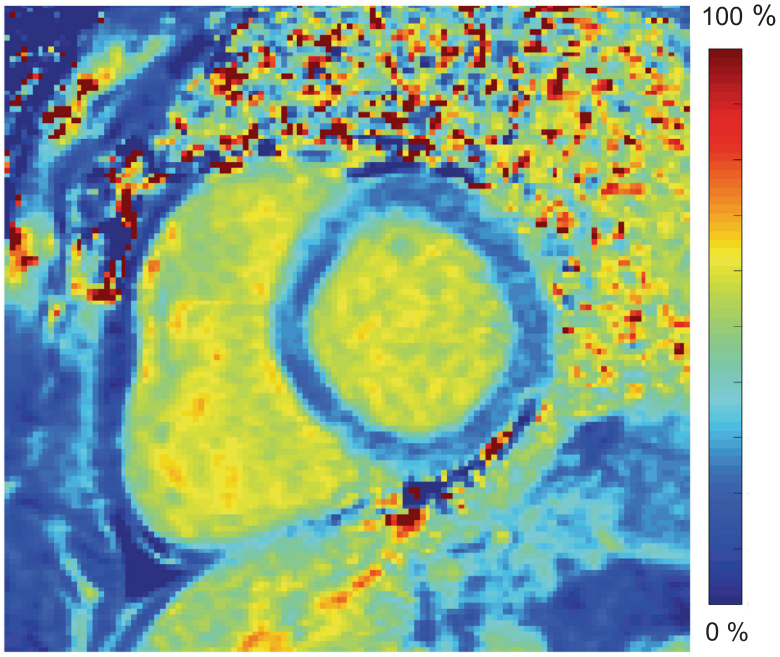

Fig. 5. ECV map generated using our software for a healthy subject.

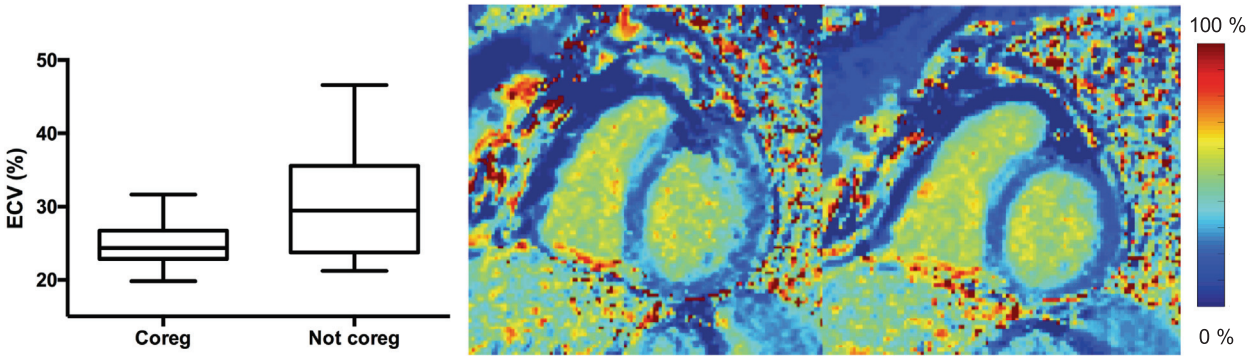

Fig. 6. On the left the box and whiskers plot shows median, 25 and 75 percentiles, and range for coregistrate versus not coregistrate ECV values for healthy subjects. Images show an example of the improvement in ECV map using image coregistration. In the central panel the non coregistered ECV map is shows while on the right the same map using image coregistration of pre- and post-contrast T1 maps is provided.

Table 3
Mean native T1, post-Gd T1 and ECV in LGE+ segments and LGE− segments. For all the maps the differences between fibrotic and non fibrotic segments is highly significant ($p < 0.001$).

	LGE+	LGE−	p-value
Native T1 (ms)	1135 ± 84	984 ± 78	<0.001
Post-Gd T1 (ms)	400 ± 31	469 ± 51	<0.001
ECV (%)	38 ± 6.7	28.5 ± 2.9	<0.001

methods is also confirmed by patient data both for pre and post contrast datasets.

A comparison between Levenberg-Marquardt algorithms and complex fitting on the T1 mapping was carried out by Barral et al. [15]. The authors found that complex fitting and the Levenberg-Marquardt algorithms were very similar in terms of accuracy. In addition to this, the complex algorithms were much faster than the Levenberg-Marquardt algorithms. In the present study, the different computational velocities of Levenberg-Marquardt and FNLS algorithms were not investigated, but we confirm the agreement between the fitting method presented and the classical Levenberg-Marquardt algorithm. Furthermore, Barral et al. [15] did not report differences in terms of accuracy between complex and magnitude fittings but they considered only the native T1 values in non-cardiac application. In our study, different T1 values were found in post-contrast blood pool values using both complex and magnitude fittings. These values were compared to MRmap output showing that magnitude fitting guaranteed accuracy at low T1 values. This different behavior of magnitude and complex fittings may be explained by the differences in the recovery curve in high and low T1 values. Because of the rapid increase in the recovery curve in short T1 tissues, post-contrast images are favored by a magnitude fitting that guarantees a more precise zero crossing, although with a slower computational velocity. Furthermore, magnitude fitting is slower than complex fitting as shown in Table 2, because the former has to compute an additional minimization process to find the zero crossing. These differences in accuracy, which apply only to *in vivo* data, are caused by movements, irregular heart rates and inhomogeneity in the magnetic field affecting the pre- and post-contrast *in vivo* T1 values in different ways. All these factors lead to differences between acquired

and fitted points, as it can be seen from the FWHM of the residuals obtained from *in vivo* data (Fig. 4).

No statistically significant differences were found between the different myocardial regions (entire myocardium, septum and lateral wall) as reported by Messroghli et al. [16] where no differences in native T1 values were detected between the cardiac segments in any of the slices (basal, medial and apical). A comparison with post-contrast values reported in the literature is of no use, because post-contrast T1 values change depending on the time elapsed from contrast injection due to individual renal and metabolic activity in the subjects. Mean ECV values in healthy subjects are in agreement with the literature [6,17,18], in particular with the values found by Kellman et al. [6] who studied a bigger sample of 62 subjects. The obtained range (mean ± 2SD) for normal myocardial ECV of 19.1%–29.9% is in close agreement with the results reported by Kellman et al., i.e. 20.4%–30.4%. In all 30 subjects, healthy volunteers and patients with a wide range of pathologies, manually extracted values correlated with automatic values. In this way, a significant correlation was found between automatic segmentation of blood pool both in pre- and post-contrast T1. This means that our binary mask efficiently distinguished blood pool related pixels thus minimizing partial volume effects and other confounding factors. Manual versus automatic myocardial ECV approach was also tested in all the subjects. The highly significant correlation between the values confirms the reliability of our maps in a wide range of ECVs (in healthy and pathological subjects).

Affine coregistration of pre- and post-contrast T1 maps is necessary to obtain reliable T1 maps. As can be seen from the example in Fig. 6, coregistration can improve the quality of the individual ECV map. Moreover, considering ECV values obtained in healthy subjects with and without coregistration, a significant difference between values and an increased CI in not co-registered maps was found. The use of coregistration algorithm in conjunction with motion corrected images leads to more reliable and robust ECV maps, as reported by Kellman et al. [6]. The advantage of ECV mapping over native T1 mapping is that it minimizes systematic errors, permits a better comparison of scans at different time points and results in less variability at different magnetic field strengths and across different vendor platforms [20]. Clinically, there is a wide spread of ECV values with overlap of values between normal and diseased myocardium. This makes it problematic for diagnostic purposes and more suited to measurement of interval changes among individuals. The capability of our T1 and ECV maps to discriminate between pathologic versus normal myocardium was proved considering the LGE positive segments. Significant differences between the maps were found comparing native and post-contrast T1values and ECV in LGE+ versus LGE− areas.

5. Conclusions

FNLS algorithm for T1 fitting is fast and robust, and reliable pre- and post-contrast T1 maps of myocardium can be obtained. The myocardial T1 values obtained in healthy subjects using our software correlate with those obtained using MOLLI sequences reported in the literature. Before starting ECV mapping, image coregistration between pre- and post-contrast T1 maps was implemented. This pre-processing step improved the quality of individual ECV maps and provided reliable ECV values with a smaller CI. The second pre-processing step is the automatic mask for blood pool extraction that provides automatic and operator independent ECV maps.

ECV mapping was implemented so that it was possible to obtain a myocardial ECV in healthy subjects in line with the literature. Furthermore, pixel-wise ECV maps obtained with this automatic method permitted a direct visualization of the extent and severity of myocardial alterations as compared to the manual approach. Furthermore, T1 mapping acquisition is increasingly available on MR scanners and this proposed tool complements myocardial tissue characterization workflow required for ECV map generation. This software is automatic and operator independent and can be a robust and powerful tool for clinicians. The possibility to intuitively visualize T1 and ECV maps in addition to the user-friendly interface can promote diffusion of this promising technique. The ECVmap tool is freely available at the following address: https://github.com/iacopo-carbone/ECVmap under the GNU General Public License (GPL) only for research purpose.

Acknowledgments

The authors would like to thank Dr Andreas Greiser for providing the MOLLI sequence, Valdo Casali and Prof. Bottari for their help in the preparation of phantoms and Karen Outtrup for linguistic revision of the manuscript.

References

[1] Constantine G, Shan K, Flamm SD, Sivananthan MU. Role of MRI in clinical cardiology. Lancet 2004;363:2162–71. doi: http://dx.doi.org/10.1016/S0140-6736(04)16509-4.

[2] Mahrholdt H, Wagner A, Judd RM, Sechtem U, Kim RJ. Delayed enhancement cardiovascular magnetic resonance assessment of non-ischaemic cardiomyopathies. Eur Heart J 2005;26:1461–74. doi: http://dx.doi.org/10.1093/eurheartj/ehi258.

[3] Galea N, Francone M, Zaccagna F, Ciolina F, Cannata D, Algeri E, et al. Ultra low-dose of gadobenate dimeglumine for late gadolinium enhancement (LGE) imaging in acute myocardial infarction: a feasibility study. Eur J Radiol 2014;83:2151–8. doi: http://dx.doi.org/10.1016/j.ejrad.2014.09.002.

[4] Carbone I, Friedrich MG. Myocardial edema imaging by cardiovascular magnetic resonance: current status and future potential. Curr Cardiol Rep 2012;14:1–6. doi: http://dx.doi.org/10.1007/s11886-011-0235-9.

[5] Burt JR, Zimmerman SL. Myocardial T1 mapping: techniques and potential applications. Radiographics 2014;34:377–95. doi: http://dx.doi.org/10.1148/rg.342125121.

[6] Kellman P, Wilson JR, Xue H, Ugander M, Arai AE. Extracellular volume fraction mapping in the myocardium, part 1: evaluation of an automated method. J Cardiovasc Magn Reson 2012;14:64. doi: http://dx.doi.org/10.1186/1532-429X-14-64.

[7] Treibel Ta, White SK, Moon JC. Myocardial tissue characterization: histological and pathophysiological correlation. Curr Cardiovasc Imaging Rep 2014;7:1–9. doi: http://dx.doi.org/10.1007/s12410-013-9254-9.

[8] Ugander M, Soneson H, Engblom H, van der Pals J, Erlinge D, Heiberg E, et al. Quantification of myocardium at risk in myocardial perfusion SPECT by co-registration and fusion with delayed contrast-enhanced magnetic resonance imaging – an experimental ex vivo study. Clin Physiol Funct Imaging 2012;32:33–8. doi: http://dx.doi.org/10.1111/j.1475-097X.2011.01051.x.

[9] Salerno M, Janardhanan R, Jiji RS, Brooks J, Adenaw N, Mehta B, et al. Comparison of methods for determining the partial coefficient of gadolinium in the myocardium using T1 mapping. J Magn Reson Imaging 2013;38:217–24. doi: http://dx.doi.org/10.1002/jmri.23875.

[10] Kellman P, Hansen MS. T1-mapping in the heart: accuracy and precision. J Cardiovasc Magn Reson 2014;16:1–20. doi: http://dx.doi.org/10.1186/1532-429X-16-2.

[11] Xue H, Shah S, Greiser A, Guetter C, Littmann A, Jolly MP, et al. Motion correction for myocardial T1 mapping using image registration with synthetic image estimation. Magn Reson Med 2012;67:1644–55. doi: http://dx.doi.org/10.1002/mrm.23153.

[12] Messroghli DR, Rudolph A, Abdel-Aty H, Wassmuth R, Kühne T, Dietz R, et al. An open-source software tool for the generation of relaxation time maps in magnetic resonance imaging. BMC Med Imaging 2010;10:16. doi: http://dx.doi.org/10.1186/1471-2342-10-16.

[13] Marquardt DW. An algorithm for least-squares estimation of nonlinear parameters. J Soc Ind Appl Math 1963;11:431–41. doi: http://dx.doi.org/10.1137/0111030.

[14] Amiri-Simkooei A, Jazaeri S. Weighted total least squares formulated by standard least squares theory. J Geodyn Sci 2012;2:113–24. doi: http://dx.doi.org/10.2478/v10156-011-0036-5.

[15] Barral JK, Gudmundson E, Stikov N, Etezadi-Amoli M, Stoica P, Nishimura DG. A robust methodology for in vivo T1 mapping. Magn Reson Med 2010;64:1057–67. doi: http://dx.doi.org/10.1002/mrm.22497.

[16] Messroghli DR, Plein S, Higgins DM, Walters K, Jones TR, Ridgway JP, et al. Human myocardium: single-breath-hold MR T1 mapping with high spatial resolution reproducibility study. Radiology 2006;238:1004–12. doi: http://dx.doi.org/10.1148/radiol.2382041903.

[17] Ugander M, Oki AJ, Hsu LY, Kellman P, Greiser A, Aletras AH, et al. Extracellular volume imaging by magnetic resonance imaging provides insights into overt and sub-clinical myocardial pathology. Eur Heart J 2012;33:1268–78. doi: http://dx.doi.org/10.1093/eurheartj/ehr481.

[18] Roujol S, Kellman P, Manning WJ, Thompson RB. Reproducibility of four T1 mapping sequences: a head- to-head comparison of MOLLI, shMOLLI, SASHA, and SAPPHIRE. Radiology 2014;272:683–9.

[19] Raman FS, Kawel-Boehm N, Gai N, Freed M, Han J, Liu C-Y, et al. Modified look-locker inversion recovery T1 mapping indices: assessment of accuracy and reproducibility between magnetic resonance scanners. J Cardiovasc Magn Reson 2013;15:64. doi: http://dx.doi.org/10.1186/1532-429X-15-64.

[20] Jellis CL, Kwon DH. Myocardial T1 mapping: modalities and clinical applications. Cardiovasc Diagn Ther 2014;4:126–37. doi: http://dx.doi.org/10.3978/j.issn.2223-3652.2013.09.03.